NanoImpact 13 (2019) 112–122

Contents lists available at ScienceDirect

NanoImpact

journal homepage: www.elsevier.com/locate/nanoimpact

Research paper

Ligands and media impact interactions between engineered nanomaterials and clay minerals

Carol A. Johnson[a,b], Margaret Chern[b], Thuy T. Nguyen[c], Allison M. Dennis[b,c,*], Jillian L. Goldfarb[a,b,d,**,1]

[a] Department of Mechanical Engineering, Boston University, Boston, MA 02215, United States of America
[b] Division of Materials Science and Engineering, Boston University, Boston, MA 02215, United States of America
[c] Department of Biomedical Engineering, Boston University, Boston, MA 02215, United States of America
[d] Department of Biological and Environmental Engineering, Cornell University, Ithaca, NY 14853, United States of America

ARTICLE INFO

Keywords:
Engineered nanoparticles
Heteroaggregation
Quantum dots
Clay
Homoaggregation

ABSTRACT

The exponential growth in technologies incorporating engineered nanomaterials (ENMs) requires plans to handle waste ENM disposal and accidental environmental release throughout the material life cycle. These scenarios motivate efforts to quantify and model ENM interactions with diverse background particles and solubilized chemical species in a variety of environmental systems. In this study, quantum dot (QD) nanoparticles and clay minerals were mixed in a range of water chemistries in order to develop simple assays to predict aggregation trends. CdSe QDs were used as a model ENM functionalized with either negatively charged or zwitterionic small molecule ligand coatings, while clays were chosen as an environmentally relevant sorbent given their potential as an economical water treatment technology and ubiquitous presence in nature. In our unbuffered experimental systems, clay type impacted pH, which resulted in a change in zwitterionic ligand speciation that favored aggregation with kaolinite more than with montmorillonite. With kaolinite, the zwitterionic ligand-coated QD exhibited greater than ten times the relative attachment efficiency for QD-clay heteroaggregation compared to the negatively charged ligand coated QD. Under some conditions, particle oxidative dissolution and dynamic sorption of ions and QDs to surfaces complicated the interpretation of the removal kinetics. This work demonstrates that QDs stabilized by small molecule ligands and electrostatic surface charges are highly sensitive to changes in water chemistry in complex media. Natural environments enable rapid dynamic physicochemical changes that will influence the fate and mobility of ENMs, as seen by the differential adsorption of water-soluble QDs to our clay media.

1. Introduction

With the global market of nanotechnology predicted to grow by 18% between 2016 and 2024 to $173 billion (Accuray Research, 2016), there is a critical need to understand and predict the potential risks of engineered nanomaterials (ENMs) on environmental and human health throughout the nanoproduct lifecycle. Quantum dot (QD) technology has received relatively little attention within the nano-risk research arena, even though its share of the global market is predicted to surpass $35 billion by 2030 (Future Markets Inc., 2018). The vast majority of this market space is occupied by optoelectronics, especially high definition QLED-TVs and monitors, with potential widespread growth in applications as varied as thermoelectrics, photoconductors, solar cells, and in vivo and in vitro imaging, sensing and labelling (Future Markets Inc., 2018). While the end-use product will dictate the potential for environmental release of QDs, health applications and manufacturing may pose a risk for QD release to the environment in pre- and post-consumer use. Research on environmental fate of QDs to date has primarily focused on examining the potential toxic effects of QD exposure to a variety of organisms (Xiao et al., 2017; Stewart et al., 2013; Wiecinski et al., 2013; Priester et al., 2009; King-Heiden et al., 2009; Domingos et al., 2011; Aruguete et al., 2010; Rocha et al., 2017; Cho et al., 2007).

The bioavailability of toxic-metal-containing QDs depends on their

* Correspondence to: A.M. Dennis, Division of Materials Science and Engineering, Boston University, Boston, MA 02215, United States of America.
** Correspondence to: J.L. Goldfarb, Department of Biological and Environmental Engineering, Cornell University, Ithaca NY 14853, United States of America.
E-mail addresses: aldennis@bu.edu (A.M. Dennis), goldfarb@cornell.edu (J.L. Goldfarb).
[1] Current address: 226 Riley-Robb Hall, Cornell University, Ithaca, NY 14853, United States of America.

https://doi.org/10.1016/j.impact.2019.01.004
Received 16 August 2018; Received in revised form 20 December 2018; Accepted 17 January 2019
Available online 18 January 2019

interactions with the surrounding environmental matrix including water chemistry, natural organic matter, and mineral particles. QDs used in biological applications (e.g., biosensing or biomedical imaging) are coated with hydrophilic organic ligands that confer solubility in aqueous solutions (Susumu et al., 2011; a Hines and Kamat, 2014; Valizadeh et al., 2012; Esteve-Turrillas and Abad-Fuentes, 2013; Delehanty et al., 2012), which could increase particle mobility in the environment. Ligand chemistry and the resultant surface properties of the nanomaterial likely play a significant role in the fate and transport of ENMs across environmental media. For example, column mobility studies on the adsorption of water-soluble QDs to sand or silty loam soil demonstrate how the QD coating charge, as well as medium pH and ionic strength, impact particle retention (Uyusur et al., 2010; Al-Salim et al., 2011). Depending on the soil type, clay minerals can comprise a significant fraction of soil matter, making it important to determine the potential influence of clays on nanoparticle mobility. Beyond soil systems, colloidal clays are present in aquatic systems, and as such it is critical to understand QD-clay behavior in aqueous media. Aggregation of nanomaterials simultaneously reduces surface area to volume effects on reactivity and as aggregate size increases the transport in porous media slows (Lowry et al., 2012). In addition to shedding light on how ENMs may move through the environment following accidental release, understanding the interactions between clays and ENMs could lead to the development of economical and efficient methods to treat aqueous QD waste to prevent such exposures. Clay minerals have historically been used in water treatment processes to remove organic and inorganic pollutants in an economically viable way (Gupta et al., 2009). Enhanced or modified clay materials are being developed for improved contaminant uptake (Gupta et al., 2009; Jiang et al., 2004; Vengris et al., 2001). By examining QD interactions with clays, the present study contributes to a body of knowledge both on aspects of the fate of aqueous QDs at the end of their life cycle and on a potential waste treatment option.

Clay minerals have variable unique elements that determine permanent and transient surface charges, presenting an intriguing, but complicated, substrate for heteroaggregation studies. The base layers consist of silicate (tetrahedral (T) arrangement of atoms) or alumina (octahedral (O) arrangement) sheets in particular patterns – TO for 1:1 clays and TOT for 2:1 clays. A constant negative charge density dominates on the T faces, which results in an electric double layer that can be neutralized by a cloud of cations (Tombácz and Szekeres, 2004; Tombácz and Szekeres, 2006). Patchy surface charge heterogeneity results with the isomorphic substitution of cations such as Al^{3+} for Si^{4+} or Mg^{2+} for Al^{3+} (Tombácz and Szekeres, 2004; Tombácz and Szekeres, 2006). Variable, pH-dependent charge occurs on edges and O faces, and can also be influenced by counterions (Tombácz and Szekeres, 2004; Tombácz and Szekeres, 2006). In this study, kaolinite (a 1:1 clay) and montmorillonite (a 2:1 clay) with their different charge structures were examined. While both kaolinite and montmorillonite exhibit dominant permanent negative charge over the entire range of pH, the montmorillonite structure includes an interlayer of water and cations that can reduce its overall negative charge and increase its cation exchange capacity. Studies examining the adsorption of cations and anions to clays have demonstrated a clear dependence on pH and ionic strength (Vasconcelos and Bunker, 2007; Sen Gupta and Bhattacharyya, 2012; Uddin, 2017), which has also been seen in a study showing that both positively-charged TiO2 and negatively-charged citrate-coated Ag nanoparticles agglomerate with montmorillonite under the right media conditions (Zhou et al., 2012).

The complex characteristics of both the nanoparticle and surrounding media (e.g., particle size, composition, surface ligand, and surface charge; solution composition, pH, ionic strength, and temperature, etc.) impact behavior. Efforts to understand nanoparticle behavior, based on primary physicochemical properties and mechanisms, are confounded by the sheer number of nanoparticle-media combinations. Therefore, 'functional assays' can be used to bridge the gap from material parameters to endpoint pollutant fate, whereby results of the assay serve to inform behavior modeling. Observed trends in the assay enable the reproducible prediction of outcomes independent of a mechanistic understanding of underlying material interactions (Hendren et al., 2015; Geitner et al., 2017). Examples of quantitative functional assay endpoints include dissolution rates, aggregation rates, and air/water distribution coefficients, with standardized experimental conditions facilitating effective comparisons (Hendren et al., 2015). Attachment efficiency (α) is a rate coefficient that can be useful in ENM risk models to describe the degree of interaction between materials. This variable can be used to describe homoaggregation and/or heteroaggregation by relating the rate of particle deposition on a collector to the rate of collisions with the collector. An α of unity suggests a "perfect" attachment efficiency whereby there are no electrostatic barriers to attachment (Barton et al., 2014; Lecoanet et al., 2004). Until recently, α has been determined using complex bottom-up calculations based on theories of particle aggregation and sedimentation (von Smoluchowski, 1917; Quik et al., 2014; Friedlander, 1977). A more simplified model that reduces the number of redundant and unknown parameters is needed to facilitate broad use in environmental fate and transport models (Quik et al., 2014). Barton et al. performed a simple mixing experiment combining nanoparticles of different composition, size, coating, and overall charge with liquid from activated sewage sludge in order to calculate removal percentages and affinity coefficients (Barton et al., 2014). This method was applied and extended to use attachment efficiencies of gold nanoparticles to algae to predict the trophic transfer of those nanoparticles up the food chain to *Daphnia magna* flies (Geitner et al., 2016). Even simple mixing experiments have been shown to be relevant for complex systems. Attachment efficiency constants were correlated almost 1:1 with constants calculated from column experiments in the case of PVP-coated silver nanoparticles and glass beads (Geitner et al., 2017), and relative trends in α calculated from glass bead assays mirrored removal rate trends from realistic aquatic mesocosms for a variety of coated and uncoated ENMs (Espinasse et al., 2018). Therefore, mixing-based heteroaggregation assays show promise for understanding nanoparticle mobility in natural and engineered aqueous environments.

In this context, we used mixing studies to probe the effects of nanoparticle coating surface charge, background particle net charge, and water chemistry on heteroaggregation metrics. We used CdSe QDs for their consistency in size, shape, and diverse ligand functionalization. Two ligands with either a negative or zwitterionic charge were used to solubilize the QDs in aqueous solution. Kaolinite and montmorillonite clays represented different charge structures of potential background collector particles. Experimental solutions varied in the ionic species present (none, monovalent, or mixed mono- and divalent in deionized water (DIW), NaCl solution (saline), and moderately hard reconstituted water (MHRW), respectively). Several ENM outcomes were observed, namely, dissolution, homoaggregation, and heteroaggregation with clay. Zeta potential by itself was an insufficient physicochemical indicator of aggregation and sorption behavior. Our results additionally caution against using DIW or even a sodium chloride saline solution as an environmental analog. Ultimately, due to complex QD behavior involving homoaggregation and/or dissolution in many of the experiments, relative affinity coefficients were only quantified for two scenarios. The mixing experiment-based functional assay to quantify α was helpful in some contexts, but not fully generalizable at this stage of experimentation.

2. Materials and methods

2.1. Chemicals

Chemicals used to synthesize quantum dots were of the highest practical quality, and are as follows: cadmium oxide (99% metals basis, Alfa Aesar), selenium (pellets < 5 mm, ≥99.99% trace metals basis,

Sigma-Aldrich), trioctylphosphine oxide (TOPO, ReagentPlus, 99%, Sigma-Aldrich), trioctylphosphine (TOP, 97%, Sigma-Aldrich), 1-octadecene (ODE, technical grade, 90%, Sigma-Aldrich), oleic acid (technical grade, 70%, Sigma-Aldrich), and oleylamine (technical grade, 70%, Sigma-Aldrich). Ligand reagents included DL-thioctic acid (≥98%, Acros Organics), 1,1′-carbonyldiimidazole (CDI, 97%, Acros Organics), ethylene diamine (≥99%, Sigma-Aldrich), methyl acrylate (≥99%, Acros Organics), lithium hydroxide (≥98%, Sigma-Aldrich), and sodium borohydride (powder, Fisher Scientific). HPLC-grade solvents were used without further purification, such as hexanes (Fisher Scientific), methanol (Honeywell), chloroform (J.T. Baker), and ethanol (Sigma-Aldrich). The clay minerals chosen for this study, kaolinite (Kaolin, USP, acid-washed powder, Fisher Scientific) and montmorillonite K10 (Alfa Aesar, reported surface area of 220–270 m^2/g), were used without further treatment. Unless noted as de-ionized (DI) water, nanopure water was used for all aqueous solution preparation (18.2 MΩ-cm Type I water, Milli-Q Reference, EMD Millipore). Salts used for aggregation experiments were of trace metal grade quality: $MgSO_4$ (≥99.99% trace metals basis, Aldrich), $CaSO_4$ (anhydrous, Puratronic 99.993% metals basis, Alfa Aesar), $NaHCO_3$ (puriss. p.a., ACS reagent, ≥99.7%, Sigma Aldrich), and KCl (99.999% trace metals basis, Acros Organics), and NaCl (> 99.5%, BioXtra, Sigma Aldrich). Concentrated nitric acid for sample acidification was trace metal grade (Fisher Scientific).

2.2. CdSe QD synthesis

CdSe quantum dots were synthesized from 0.2 M cadmium oleate ($Cd(OA)_2$) and 1 M trioctyl phosphine selenide (TOP:Se) following an established method (Ghosh et al., 2012; Chern et al., 2017). 1 M TOP:Se was prepared by dissolving the appropriate amount of selenium pellets directly into TOP by stirring overnight at 60 °C in an argon environment glovebox. 0.2 M $Cd(OA)_2$ was made in a 1:4 cadmium to oleic acid ratio by first dissolving cadmium oxide directly into oleic acid at 150 °C under vacuum and then further diluting with ODE to achieve a concentration of 0.2 M. The cadmium precursor was heated to 80 °C and degassed before use. For nucleation of CdSe QDs, 2 g TOPO, 16 mL ODE and 3.7 mL of 0.2 M $Cd(OA)_2$ were loaded into a 100 mL round bottom flask. The solution was held under vacuum for 30 min at room temperature before heating to 80 °C and further held under vacuum for another 30 min. After evacuating for an hour, the flask was put under argon and heated to 300 °C. During the evacuation of the cation precursor, 1.52 mL of 1 M TOP:Se, 6 mL of oleylamine, and 2 mL of ODE were mixed and loaded into a syringe inside of a glovebox. The Se precursor mixture (9.5 mL total) was injected into the Cd mixture at 300 °C and the reaction removed from the heating mantle and allowed to cool to room temperature after 3 min. Cores were stored at 4 °C. For further use, cores were precipitated with ethanol and methanol and redispersed in hexanes or chloroform.

2.3. CL4 ligand synthesis and exchange onto CdSe QDs

A double batch of the zwitterionic bidentate ligand “compact ligand four” (CL4) was synthesized following the method of Susumu et al. (2011) with minor modifications as described fully in Chern et al. (2017). Intermediate compounds were purified using flash column chromatography (Teledyne ISCO CombiFlash Rf + UV–Vis) using columns packed with 63–200 μm silica gel (Dynamic Adsorbents, Inc). To exchange the TOP/TOPO/ODE ligands on the QDs with CL4, a biphasic mixture of QDs in chloroform and CL4 in DIW (108.6 mmol CL4/μmol QDs) was vigorously stirred in argon-filled glass vials in the dark overnight. The water phase containing QDs was collected, filtered through a 0.1 μm PVDF syringe filter (Celltreat Scientific Products LLC) and buffer exchanged three times with nanopure water using a 30 kDa centrifugal filter (EMD Millipore Amicon). CdSe-CL4 QDs were stored concentrated at 4 °C.

2.4. CdSe-MPA preparation

CdSe-MPA QDs were purchased from Ocean Nanotech (#QCH-580-50) in powdered form and prepared freshly each day of use. First, they were ground using a mortar and pestle and the finest particles were suspended in nanopure water. The suspension was vortexed, sonicated briefly, and centrifuged to remove large aggregates. Centrifugal filtration (EMD Millipore Amicon, 10 kDa pore size) was used to concentrate the suspension.

2.5. Matrix solutions

The EPA standard moderately hard reconstituted water (MHRW) was prepared from 0.06 g/L $MgSO_4$, 0.05 g/L $CaSO_4$, 0.096 g/L $NaHCO_3$, and 0.004 g/L KCl in nanopure water (United States Environmental Protection Agency, 2002), with an ionic strength of 4.6 mM. A solution of 4.7 mM NaCl (0.03% w/v) in nanopure water was prepared and is referred to as saline throughout the text. DIW was used as the third matrix solution. The pH of each solution was measured with pH paper (accuracy of $+/-0.2$ pH units) for quick checks during aggregation studies, and validated with a pH meter (ThermoScientific Orion Star A211) in separate experiments examining the effect of the clays and QDs on the matrix pH.

2.6. Material characterization

The size and concentration of raw and water-soluble quantum dots were calculated from the wavelength and intensity of the 1S peak measured by UV–Vis spectrophotometry (Thermo Scientific Nanodrop 2000c) using established empirical formulas correlating the QD absorption features with particle diameter and molar extinction coefficient (Yu et al., 2003) and the Beer-Lambert Law. The CdSe core radius value obtained from the 1S peak wavelength was used along with the density of wurtzite CdSe (5.81 g/cm^3) and an assumption of a 1-to-1 Cd-to-Se elemental ratio to obtain the molar mass of the QD. To calculate the initial Cd and Se concentrations in the experimental solutions, a Cd/Se ratio of 1.2 was used because there are excess Cd atoms on the nanoparticle surface (Taylor et al., 2001).

The zeta potential (ZP) of QD and clay in each matrix solution was measured using a Malvern Zetasizer NanoZS. QD samples were prepared by diluting 20 μL of QD stock in nanopure water into 800 μL of matrix solution (DIW, saline, or MHRW). Clay samples were prepared by allowing 0.6 g/L suspensions of kaolinite and montmorillonite in each of the three matrices to settle overnight before an aliquot of the supernatant was used for analysis. The pH of these clay suspensions was also measured (ThermoScientific Orion Star A211).

Cation exchange capacities (CEC) for kaolinite and montmorillonite were obtained using the ammonium acetate (NH_4OAc) method (Unuabonah et al., 2013). Briefly, 0.02 g of clay was added to 5 mL of 0.5 M NH_4OAc solution, agitated for 6 h on a horizontal shaker table, filtered, and the filtrate kept for ICP-MS analysis of Na^+, K^+, Ca^{2+}, and Mg^{2+}. The concentration of each cation in meq/mol was calculated by the following equation

$$Exchangeable\ Cation = (aVc)/(10Ms) \quad (1)$$

where a is the concentration of cation from extract solution, c is the moles of equivalent charge per mol of ion, V is the volume of NH_4OAc, M is the molar mass of the cation, and s is the clay mass. The cation exchange capacity is the summation of the four exchangeable cations.

In order to determine accurate Cd/Se ratios and to verify the relationship between [QD], [Cd] and [Se], a dilution series of CdSe-CL4 was analyzed by UV–Vis (Agilent Cary 5000). An aliquot of each was then digested with concentrated HNO_3 and heated for 25 min in a 60 °C water bath to ensure complete digestion of the QDs. The resulting digestate was diluted to 2% HNO_3 in nanopure water and analyzed by ICP-MS (Agilent 7800) in He and high energy He modes for Cd and Se

concentrations, respectively. The consistency of Cd/Se for each batch of CdSe cores was also confirmed by digestion in HNO_3 followed by ICP-MS analysis. During ICP-MS analyses, a blank and a second source calibration standard were run approximately every 10–15 samples to monitor for instrument drift. All tuning and calibration solutions were purchased from High Purity Standards. Minimum detection limits calculated on the basis of calibration method blanks (MDL_B) (United States Environmental Protection Agency, 2016) were 0.38 ppb for Cd and 0.13 ppb for Se. Experimental method blanks were consistently below these values.

2.7. Experimental setup

Eight 45-min kinetic experiments were performed in triplicate with a clay mineral and a clay-free control on the same day. QDs were added at a final concentration of 13 mg/L to 8 mL of matrix solution in an acid-washed 3-dram glass vial with mixing via stir bar at 400 rpm. To start the experiment, an aliquot of pre-equilibrated, sonicated clay in the matrix solution was added to a final concentration of 300 mg/L. Aliquots of 300 µL were sampled just before the clay was added ($t = 0$) and at specific time intervals after clay addition, centrifuged for 30 s at 2000 rcf (Fisherbrand Standard Mini Centrifuge) to separate the sorbed and suspended QDs. 200 µL of the supernatant were removed and passed through a 0.2 µm PVDF syringe filter (Restek). This filtration step was necessary to prevent stray clay particles from clogging the ICP-MS nebulizer. 200 µL of concentrated HNO_3 was added overnight to dissolve the QDs, then diluted to 2% HNO_3 in nanopure water. Elemental concentrations (Cd, Ca, Mg, Na, and K) were measured with ICP-MS (Agilent 7800) in helium mode, while Se was analyzed in high energy helium mode in order to eliminate the interference of the Ar-Ar dimer at mass 78.

Initial Cd and Se concentrations calculated from the initial QD concentration (via UV–Vis) were used to normalize the Cd and Se remaining in solution. Cd and Se removal fractions were then obtained using:

$$(C_r/C_i) = 1–(C_t/C_i) \quad (2)$$

where C_r = concentration of Cd or Se removed, C_i = initial calculated Cd or Se concentration before the addition of clay, and C_t = concentration at time t. The value of C_r/C_0 at $t = 0$ represents the QDs that were removed by centrifugation and syringe filtration absent the addition of clay. Kinetic experiments without clay were also performed to monitor colloidal stability with regard to dissolution and homoaggregation, and are plotted separately from clay experiments. Cd/Se molar ratios were calculated directly from the Cd and Se concentrations in the experimental solution. Reported standard deviations were calculated based on triplicate experimental values for experiments with clay, and were consistently greater than or equal to the error propagated from the ICP-MS measurement errors.

2.8. Speciation modeling

Water chemistry and ion speciation modeling for each experimental setup (including clay-free controls) was performed using the free and open-source software PHREEQC Interactive (v.3.4.0 for Windows), distributed by the U.S. Geological Survey. pH was allowed to equilibrate to achieve charge balance. O_2 and CO_2 gasses were equilibrated to log partial pressures of −0.68 and −3.5, respectively. A measure of redox potential, pe, was determined from the equilibrium of $O_{2(g)}$. Solid phase CdSe, kaolinite, Na-montmorillonite, and Ca-montmorillonite were added to the model as equilibrium phases with saturation indices of 0. Models utilized thermodynamic data from the minteq.v4 database for CdSe and kaolinite, and from the llnl database for Na- and Ca-montmorillonite phases. Relevant outputs from this model included changes in pH due to the addition of solid phases, ionic strength calculations, and ion speciation.

MPA and CL4 ligand charge speciation across the pH range was modeled using the Protonation plugin in MarvinSketch (v. 16.10.10, ChemAxon) and the following parameters: micro mode (less than eight ionizable species), temperature of 298 K, no corrections, and tautomerization/resonance were considered. Because the ligands were bound to the QDs by their thiol groups, any results for species involving de-protonated sulfur were removed, and the total percentages for the variants of each of the other functional groups (e.g., carboxylic acid and carboxylate) were adjusted to sum to 100% at any given pH.

2.9. Heteroaggregation attachment efficiency calculations

For systems in which heteroaggregation dominates the initial nanoparticle removal kinetics by the larger background particles (clays, in our case), a simple relationship exists between the concentration of nanoparticles (initial calculated QD_i and QD_t at time t), attachment efficiency coefficient (α), the concentration of background particles (B), and the collision frequency between the nanoparticles and background particles (β): (Geitner et al., 2017; Barton et al., 2014; Geitner et al., 2016)

$$ln(QD_i/QD_t) = \alpha\beta Bt \quad (3)$$

The natural log of the inverse ratio of QD concentration at time t to the initial concentration (equivalent to the Cd or Se concentration ratio) was plotted versus time; for samples exhibiting a linear relationship, the slope is equivalent to $\alpha\beta B$. Knowledge of both B and β is necessary to calculate α; B is known for our system, but additional experiments where all particles aggregate (i.e., $\alpha = 1$) would be required to calculate β. We assume that β is constant between our experiments due to consistent mixing speeds. Thus, in this paper we report the combined $\alpha\beta B$, to compare relative attachment efficiencies.

3. Results and discussion

We hypothesized that the surface properties of water-soluble nanoparticles, the exposed charge of clays, and the pH and ionic strength of the surrounding aqueous media all influence the complex interactions between ENMs and their surroundings. We tested this hypothesis by examining the homo- and heteroaggregation of semiconductor quantum dots with two distinct surface coatings in three different aqueous media of increasing complexity, in the presence or absence of two different clay compositions. Careful characterization of the individual components and their interactions form the basis of our conclusions.

3.1. Characterization of QDs, clays, and their suspensions

The position of the QD 1S peak, obtained by UV–Vis spectroscopy, is listed in Table 1 for each of the QD samples used. The 1S peak position was used to determine the particle core diameter, molar mass, and molar extinction coefficient, as previously described (Yu et al., 2003).

The stock solutions of DIW, MHRW (a standard simulated freshwater), and a saline (NaCl) solution of the same ionic strength as MHRW were chosen to show the importance of including environmentally relevant chemistries in experiments. The combination of mono- and divalent cations in MHRW, at a relevant pH, is more

Table 1
Characterization of QDs by UV–Vis.

	1S peak (nm)	Core diameter (nm)	Core molar mass (g/mol)	ε[a] (L/mol/cm)
CdSe-CL4	572	3.58	84,055	171,177
CdSe-MPA	560	3.26	53,594	134,113

[a] ε: Molar extinction coefficient.

Table 2
pH, zeta potential (ζ) and conductivity (σ) measurements for QDs and clays in experimental solutions.

	Stock solution	CdSe-MPA	CdSe-CL4	Kaol	Mont
DIW					
pH	5.43			5.77	9.90
ζ (mV)[a]		−23.2 (0.8)	−18.4 (1.6)	−37.2 (0.6)	−33.8 (0.4)
σ (uS/cm)[a]		14.8 (5.7)	11.2 (7.5)	2.1 (0.2)	91.1 (1.4)
Saline (4.7 mM NaCl)					
pH	4.96			5.53	9.86
ζ (mV)		−28.3 (1.0)	−11.5 (0.3)	−39.6 (0.4)	−34.0 (0.4)
σ (uS/cm)		550 (5)	533 (4)	580 (16)	623 (16)
MHRW					
pH	7.93			8.13	8.90
ζ (mV)		−19.2 (0.4)	−29.0 (1.3)	−25.4 (0.5)	−19.8 (0.2)
σ (uS/cm)		303 (2)	294 (2)	285 (8)	334 (5)

[a] ζ and σ averages (with standard deviations) were calculated from n = 4–6 measurements for the clay samples and n = 3 for the QD samples.

representative of the interactions with particle surfaces and influences on overall charge balances than DIW (ion-free). Since our solutions were not buffered, careful measures of solution chemistry changes in different conditions (Table 2) were compared with water chemistry and speciation modeling (Table S1 in the ESI). Kaolinite increased the pH by 0.2–0.6, and montmorillonite increased the pH by 1–4.9 (Table 2). The increase in pH upon clay addition was close to expected values for kaolinite, for which water chemistry models predicted a pH increase of 0.1 (Table S1). In contrast, the measured increase in pH was much larger than the maximum 0.8 pH unit increase predicted upon the addition of montmorillonite (for both Na and Ca versions) to DIW or saline. The model indicated that the buffer capacity of MHRW would prevent changes in pH upon the addition of clay (Table S1), but the addition of montmorillonite still increased the measured pH by 1. One possibility for the large discrepancy for montmorillonite is that it was not acid-washed and may have contained other constituents that affected the pH, unlike kaolinite, which came acid-washed from the supplier. QDs themselves had a negligible contribution to the solution pH when added to the matrix solution (Table S1), and therefore the pH of the stock solution can be assumed to also hold true for the QD zeta potential measurements. Overall, with the exception of montmorillonite samples at pH 9.9 in DIW and saline, experimentally measured pH values were similar to values modeled using PHREEQCi.

Modeling of the QD ligand charge speciation from pH 4 to 10 resulted in calculated pK_as for CL4 that match well with reported values calculated with alternative software (Fig. 1). Specifically, the pK_as of the two carboxylic acid groups are 2.9 (3.29 (Susumu et al., 2011)) and 3.6 (3.93 (Susumu et al., 2011)), and the tertiary amine is 9.0 (9.06 (Susumu et al., 2011)). The pK_a of the carboxylic acid group in MPA was calculated to be 4.6 (4.34 (National Center for Biotechnology Information, n.d.; Patty, 1963)). An increase in the actual pK_a of the ligand attached to the QDs can result from an increase in nanoparticle size, increase in background cations, and increase in cation size (Wang et al., 2011). Based on the pK_as for free ligands, CL4 exists almost exclusively as the zwitterion at the pH of the kaolinite suspension, but at the higher pHs of the montmorillonite suspensions, 50% or more of the tertiary amines are not protonated. This difference plays a role in the mixing experiment results, as we show below.

Zeta potential was used as an indication of the net charge for both ligand-coated QDs and clays in each matrix solution (Table 2) and is reflective of the pH and presence of counterion interactions in each solution. Ligand speciation and water chemistry modeling was useful to explain zeta potential trends. The CdSe-MPA was more negative than

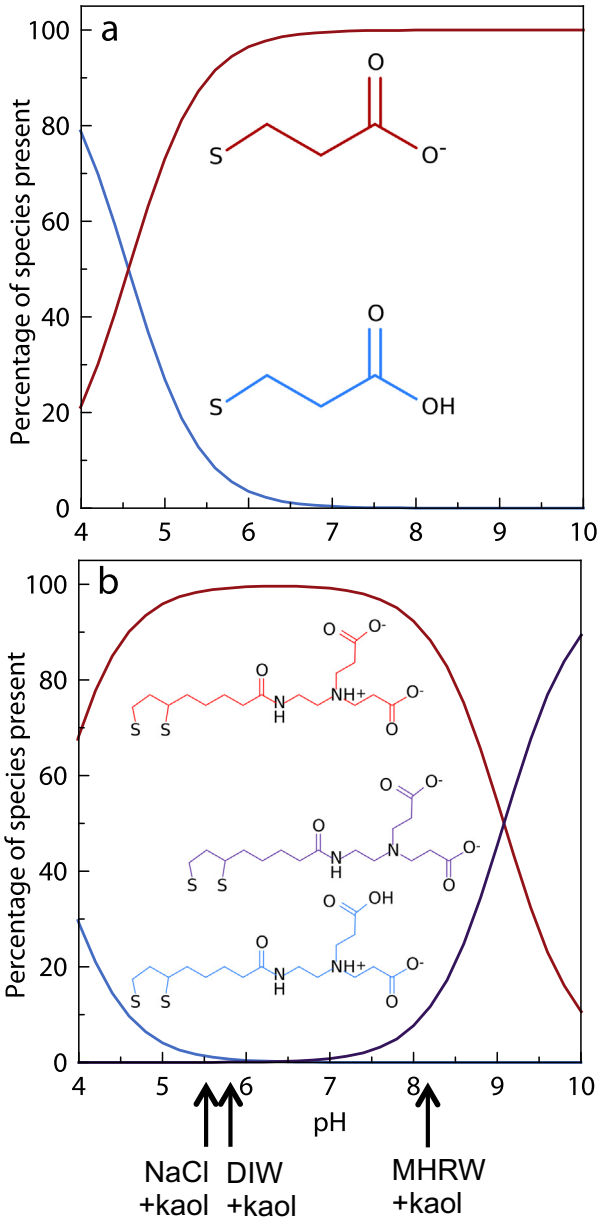

Fig. 1. Speciation of (a) MPA and (b) CL4 ligands across the pH range of 4 to 10. Sulfur species were ignored as they are bonded to the QD. Arrows indicated the measured pH of each of the aqueous solutions after the addition of kaolinite.

CdSe-CL4 in DIW and saline, but not in MHRW. At these pHs, the carboxylic acid group on the MPA ligand is negative. However, the presence of divalent cations such as Ca^{2+} are likely to partially neutralize the negative charge on the COO^- group (Shambetova et al., 2016), even more so than monovalent cations especially when present with Mg^{2+} (Chen et al., 2017), as was the case in MHRW. At pH ~5, CL4 is zwitterionic, yet in MHRW, pH 8, the CdSe-CL4 was significantly more negative than in both DIW and saline. One contribution to this more negative charge is that amine groups are neutralized as the pH approaches the pK_a, though this only accounts for about 5% of the ligand species (Fig. 1). However, there are also divalent cations available to neutralize the negative charges, as with MPA. Speciation modeling with PHREEQC showed that 90% of Ca and 92% of Mg exist as hydrated divalent cations, while only 8% of Ca and 7% of Mg are tied up in neutral compounds with sulfate (Table S1). Shifts in actual pK_a due to counterion size and the ligands being bound to nanoparticles (Wang et al., 2011) also do not account for this discrepancy. These results

confirm what is becoming common practice – that while modeling can be helpful, given the difficulty of modeling the combined effect of every species interaction in simplified and more complex systems, the zeta potential should be measured in all relevant media before making predictions about nanoparticle behavior.

The cation exchange capacity (CEC) of the clays measured 2 meq/100 g and 141 meq/100 g for kaolinite and montmorillonite, respectively. As expected, the zeta potential of montmorillonite was less negative than kaolinite in all solution matrices (Table 2) because the cations in the montmorillonite interlayers balance the permanent negative structural charges. This effect was somewhat muted due to the higher pH in DIW and saline. Zeta potentials for both clays were the least negative in MHRW, again due to both the presence of divalent cations playing a larger role in overall charge neutralization and the presence of a higher relative pH. Saline resulted in a slightly more negative zeta potential than DIW, which has been shown by Yukselen and Kaya (2003), and could be related to more positive charges on edges and O faces at the slightly higher pH (Tombácz and Szekeres, 2006).

The conductivity of each solution is related to the ionic strength and total dissolved solids, and was measured as a check on the comparability of the saline and MHRW solutions (Table 2). DIW has low conductivity due to the lack of ions present, and the addition of kaolinite or QDs has a minimal impact on this value. Montmorillonite does increase the conductivity, likely due to the outward diffusion of divalent interlayer cations. In 4.7 mM NaCl, the conductivities of the QDs or clays are 1.8–2 times higher than in MHRW, despite having the same overall ionic strength, due to a higher concentration of total dissolved solids. The presence of alkaline earth elements also results in the formation of neutral complexes with the sulfates and carbonates in MHRW (Table S1), especially at a pH approaching 9 (Miller et al., 1988), reducing the concentration of free ions. Speciation simulations using PHREEQC show that the combined effect from this charge neutralization and pH difference leads the ionic strength of MHRW to be approximately 10% lower than 4.7 mM NaCl (Table S1). The pH difference itself contributes approximately 0.05 mM to the ionic strength.

3.2. Dissolution of QDs in control experiments

An important result in these kinetic experiments using CdSe QDs, unlike Au or Ag nanoparticles, is that under some conditions the QDs are susceptible to dissolution. Since the published Cd/Se ratio for intact CdSe QDs of 1.2 ± 0.1 (Taylor et al., 2001; Jasieniak et al., 2009; Jasieniak and Mulvaney, 2007) was experimentally confirmed for CdSe-CL4 using acid digestion and ICP-MS, deviation from this value signals at least partial QD dissolution. Fig. 2 shows Cd/Se molar ratios over time for the control experiments. CdSe dissolution is thermodynamically favorable if the protective ligand coating detaches, as the saturation index of CdSe in all experimental conditions is around −73 (undersaturated, Table S1). The highly oxic conditions in these experiments favor the oxidation of Se^{2-} to Se^{6+} once bare QD surfaces are exposed (Table S1), which would lead to QD structural disruption and potential dissolution. Dissolution could also be facilitated by the presence of metal chelators such as Cl^- and HCO_3^-.

The Cd/Se ratios remain relatively stable for CdSe-MPA in saline, though only one of the saline experiments exhibited a Cd/Se of 1.2 (Fig. 2). In DIW, the solution was initially Cd-rich, but over time became Cd-poor (Se-rich). As with homoaggregation, monodentate ligands such as MPA are more prone to detachment and subsequent surface exposure than bidentate ligands such as CL4.

CdSe-CL4 exhibited minor fluctuation in Cd/Se in both saline and DIW, but was generally stable against dissolution. CdSe-CL4 in the simulated natural water, MHRW, however, exhibited an initial Cd/Se around 3, fluctuated strongly throughout the experiment and stayed high at around 2.3 after 45 min. Paydary and Casanova found that for CdSe/ZnS QDs stabilized with mercaptoundecanoic acid, the dissolution kinetics in river water at pH 6.9 were much faster than for buffered water (pH 7) and "tentatively attributed" these results to Cl^-, HCO_3^-, or organic ligands present in natural waters (Paydary and Larese-Casanova, 2015). In our geochemical simulations, 11% of Cd could complex with HCO_3^- in the form of $CdHCO_3^+$ (Table S1).

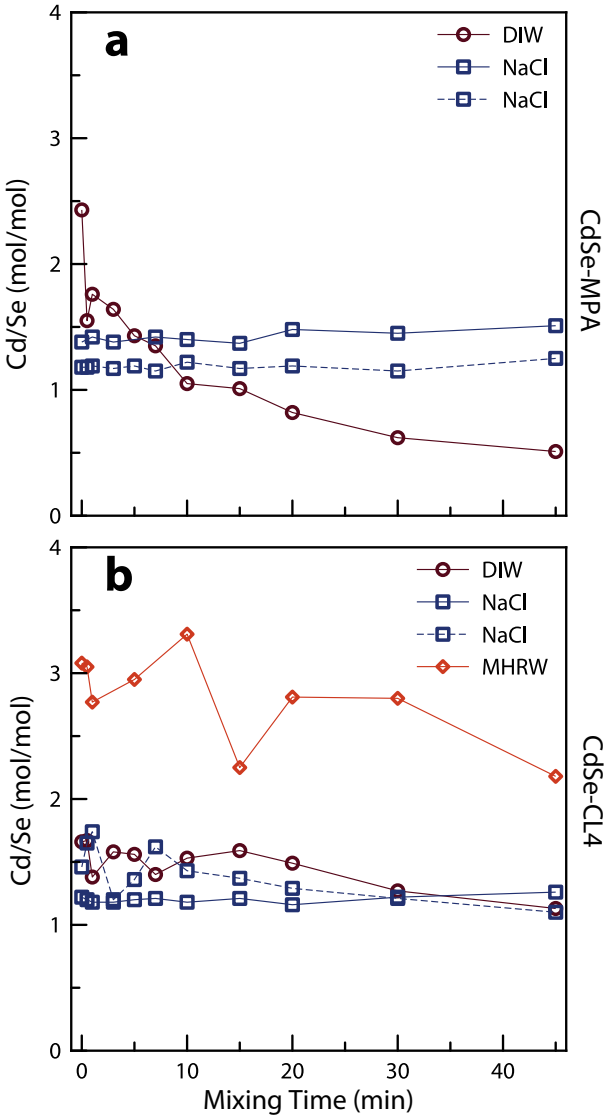

Fig. 2. Average Cd/Se molar ratios in solution after centrifugation/filtration without clay present. The Cd/Se for intact CdSe QDs is 1.2. (a) CdSe-MPA, (b) CdSe-CL4.

Similar to the control experiments, QD dissolution is evident in some conditions in the presence of clays, as indicated by deviations in the Cd/Se ratios from 1.2. Fig. 3 shows Cd/Se molar ratios for CdSe-MPA and CdSe-CL4 experiments, which generally follow the same behavior as their respective control experiments in Fig. 2. Ratios for CdSe-MPA in solution vary from Cd-rich to Se-rich, with CdSe-MPA in saline with kaolinite exhibiting the most stability. At short times (< 15 min), CdSe-CL4 is stable in saline with either clay. With kaolinite, the Cd/Se ratio drops considerably after 15 min; this behavior was not present in the corresponding control experiment. The presence of clay particles provides a negatively charged surface for the sorption of Cd^{2+}, resulting in a decrease in solution Cd/Se. The zeta potential of kaolinite was more negative than montmorillonite across all three solution types.

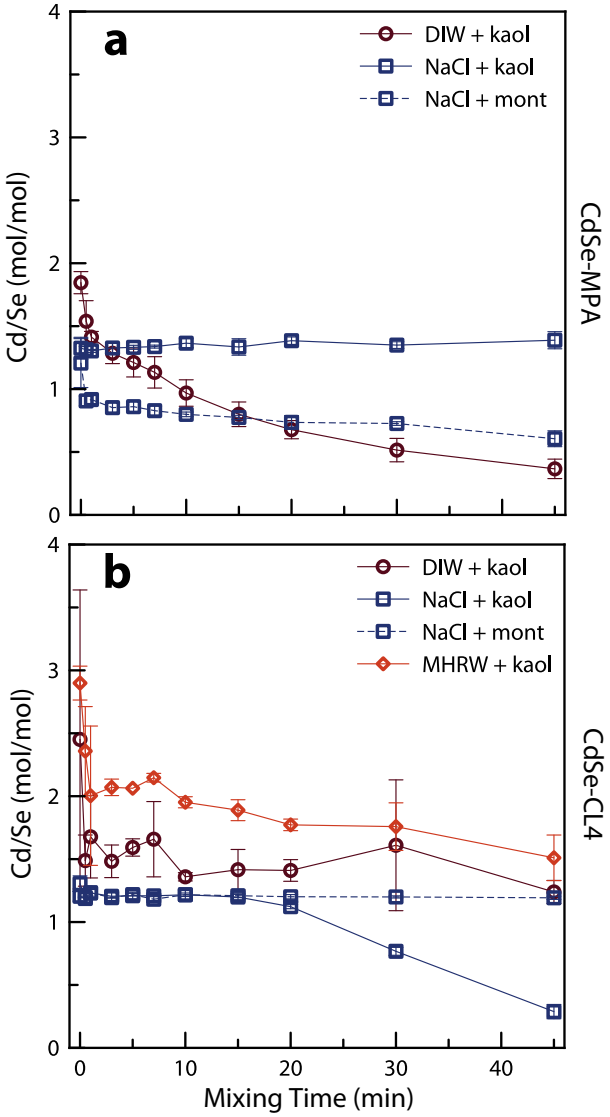

Fig. 3. Average Cd/Se molar ratios remaining in solution in the presence of clay. The Cd/Se for intact CdSe QDs is 1.2. (a) CdSe-MPA, (b) CdSe-CL4. Data presented are means ± standard deviations from triplicate experiments.

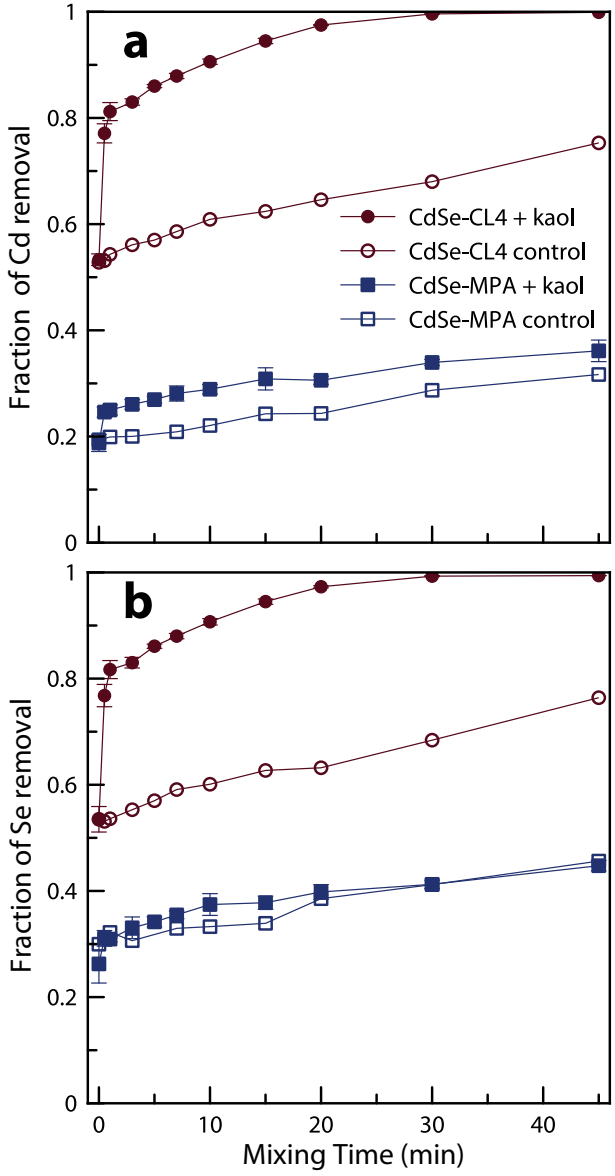

Fig. 4. Comparison between experiments in saline with and without kaolinite present, showing consistent starting points for each type of QD. Under these conditions, QDs did not appreciably dissolve. Data presented for clay experiments are means ± standard deviations from triplicate experiments, though some error bars are not visible because they are smaller than the data point.

3.3. Aggregation kinetics of intact CdSe particles

The aggregation kinetics of the QDs that remain intact with or without the clay present are shown in Fig. 4 in the form of Cd and Se removal. In paired experiments in saline with and without kaolinite, both CdSe-MPA and CdSe-CL4 persist as intact particles, as well as CdSe-CL4 with montmorillonite (shown in Fig. S1 and discussed in Section 3.5). One clear trend is that initially, before clay is added (if applicable), the fraction of QDs removed via centrifugation and filtration is > 2.5 times higher for CdSe-CL4 than CdSe-MPA. The effect of zeta potential (−11.4 and −28.3, respectively) is clearly dominating over ligand strength (bidentate vs. monodentate) in this case.

As expected, the Cd and Se removal increases rapidly after kaolinite is added to the mixing solution (Fig. 4). The removal (net aggregation) rate then slows, though cumulative net aggregation continues to increase. In the case of CdSe-CL4 and kaolinite, 100% of the CdSe is aggregated within 30 min. Aggregation kinetic theory states that initially particle breakup is negligible (Barton et al., 2014). After that, the kinetics reflect a combination of QD hetero- and homoaggregation and reverse processes. Since the kinetics between control and clay experiments are approximately parallel, the difference between the two at any given time represents the QD removal influenced by kaolinite. After 15 min of mixing, the fraction of CdSe-CL4 removed by kaolinite was approximately 5 times that of CdSe-MPA.

The effect of dilution, ionic strength, and charge neutralization by cations may all contribute to homoaggregation of QDs in the varying matrices and over time as found in the clay-free control experiments. Thiol-bonded ligand coatings are susceptible to detachment during dilution, causing the QDs to be less water soluble and aggregate (Mulvihill et al., 2010). Results from a study comparing the critical coagulation concentration of CdSe-MPA and ligands with longer chain lengths found that QDs with MPA were the least stable and started aggregating within 100 min, a result that was fully prevented by the addition of 10 mM excess ligand (Mulvihill et al., 2010). In the present study, it was necessary to use CdSe-MPA suspensions immediately after they were prepared, as within 24 h homoaggregation was evident in the form of visible flocculation (data not shown). In contrast, there were no visible signs of aggregation, instability, dissolution, or insolubility in

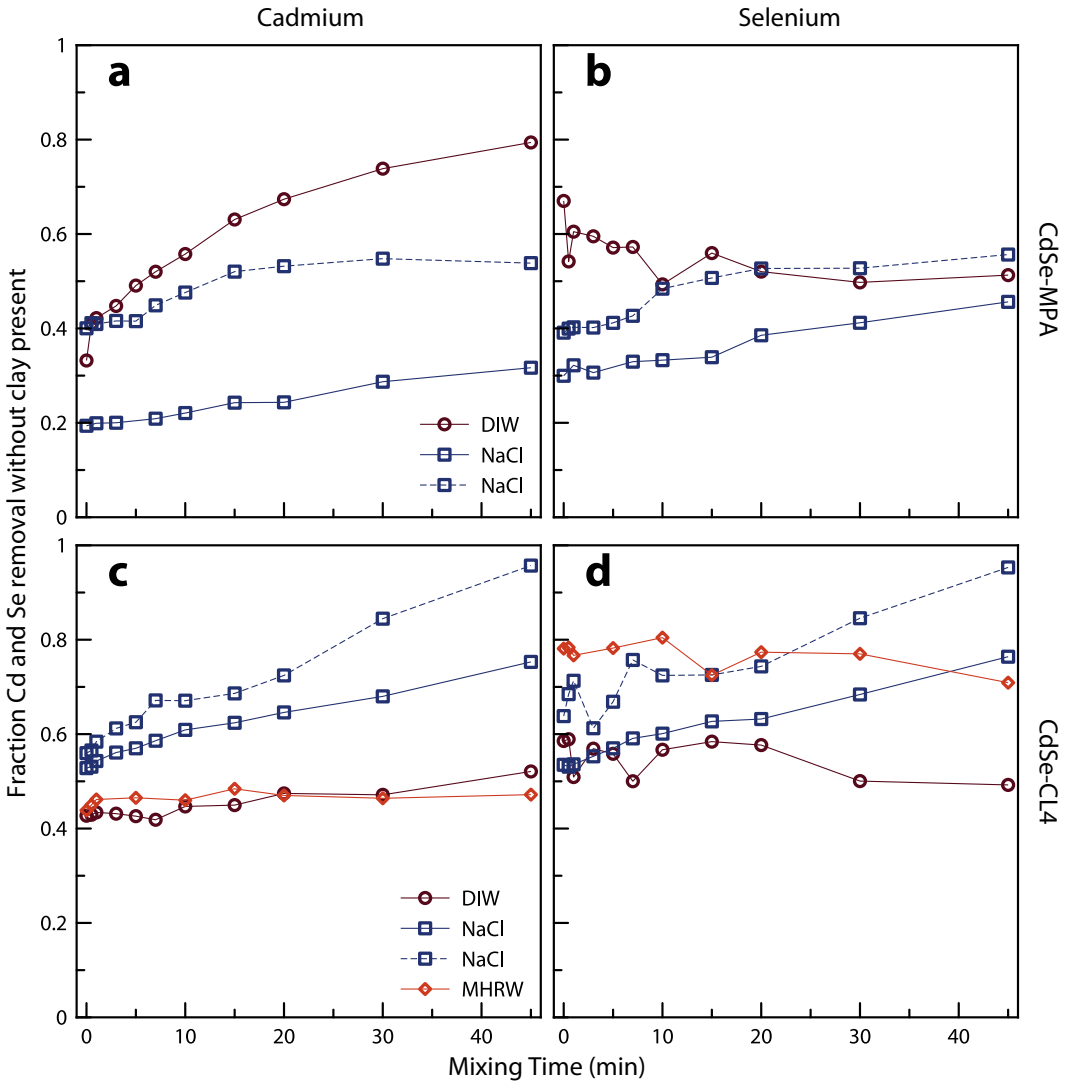

Fig. 5. Fraction of Cd and Se removed from suspension without clay present. (a) Cd from CdSe-MPA, (b) Se from CdSe-MPA, (c) Cd from CdSe-CL4, (d) Se from CdSe-CL4. The replication of experiments in saline (NaCl) without clay present represent controls correlating with kaolinite (solid line) and montmorillonite (dashed line) experiments, performed on separate days.

the stock suspension of CL4-coated QDs a month or more following the ligand exchange. This supports the conclusion that multidentate thiols are more stable against ligand detachment than monothiols (Zhang and Clapp, 2011).

CdSe-CL4 did exhibit homoaggregation in saline, despite being more resistant to ligand detachment. Charge neutralization by soluble cations can cause subsequent collapse of the electronic double layer surrounding the particles, per Derjaguin-Landau-Verwey-Overbeek (DLVO) theory (Butt et al., 2006; Verwey and Overbeek, 1948; Derjaguin and Landau, 1941). Indeed, the zeta potential of CdSe-CL4 was less negative than CdSe-MPA in saline.

3.4. Cd and Se behavior in control experiments

Fig. 5 shows the fractions of Cd and Se removed from suspension in the control experiments. Duplicate control experiments in saline were performed on different days, corresponding to kaolinite and montmorillonite experiments, but Cd and Se removal was not consistent between those duplicates despite similar experimental conditions. There are no trends with the type of matrix solution that were comparable between MPA- and CL4-coated QDs. As we saw in Fig. 2, under some conditions QDs behave like particles and some have independent Cd and Se behavior. Removal of Cd increased over time for most cases except for CdSe-CL4 in DIW and MHRW. Se behavior, on the other hand, was somewhat erratic and could be caused by the (reversible) sorption of selenate anions on any available surface such as the sides of the vials, centrifuge tubes, and syringe filters.

3.5. Cd and Se behavior in the presence of clay

Fig. 6 shows the removal fractions of Cd and Se in the presence of kaolinite or montmorillonite over time. Experiments with kaolinite in saline were discussed in Section 3.3. While the Cd/Se data for CdSe-CL4 mixed with kaolinite in MHRW show evidence for some dissolution (Fig. 2), the kinetics data show that Cd and Se have smooth removal curves with initially higher removal rates that decrease over time as almost all Cd and Se are removed from suspension. On the other hand, for CdSe-CL4 mixed with kaolinite in DIW, Cd and Se removal rates are generally constant and removal does not stabilize within the 45 min of mixing. For CdSe-MPA, Cd and Se have completely opposite behavior in DIW. Cd follows a smooth removal curve reminiscent of intact particle behavior, while Se appears to be added back into the solution over time (less removal) after initially being removed at 20% higher amount than Cd. Dissolution and dynamic sorption/desorption processes are likely

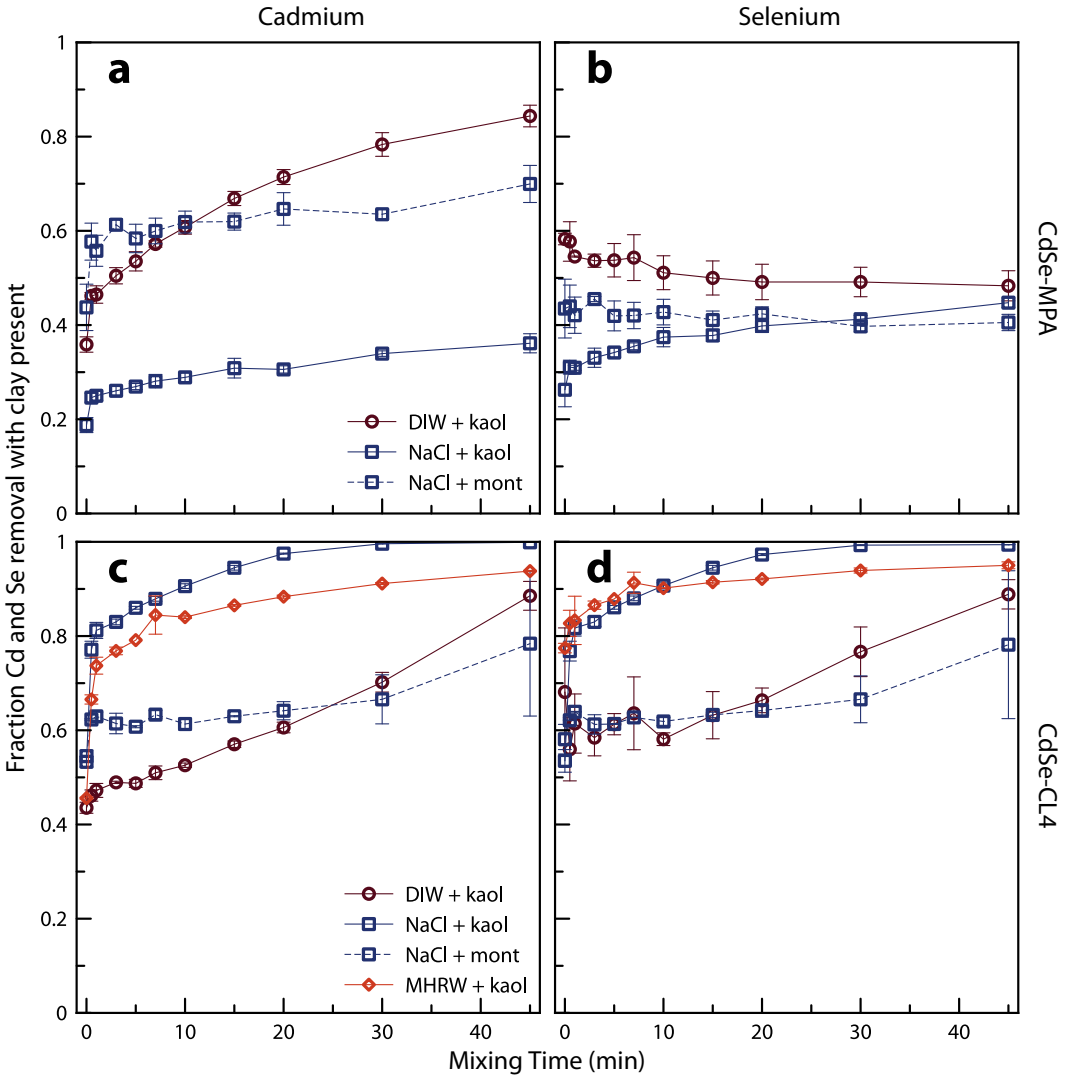

Fig. 6. Fraction of cadmium and selenium removal in the presence of clay. (a) Cd from CdSe-MPA, (b) Se from CdSe-MPA, (c) Cd from CdSe-CL4, (d) Se from CdSe-CL4. Data presented are means ± standard deviations from triplicate experiments.

acting on the Se, while the Cd is staying in the QD.

Unlike in the control experiments, CdSe-CL4 QDs mixed with montmorillonite in saline act as intact particles. After 20 min of mixing, the fraction of CdSe-CL4 removal was about 1.6 times greater with kaolinite than with montmorillonite, despite that a slightly more negative zeta potential of kaolinite in saline. Except for Cd removal involving CdSe-MPA, experiments with montmorillonite added had lower Cd and Se removal fractions than their respective controls (Fig. S1 in the ESI). Adding montmorillonite to saline caused a drastic change in pH from slightly acidic to basic (Table 2), which in turn would cause more ligands to be negatively-charged (Fig. 1) and reduce the aggregation with the very negative montmorillonite (Table 2) and themselves. The pH change happens after the initial samples were taken ($t = 0$), and so does not affect the initial removal fractions.

3.6. Evaluation of applicability of heteroaggregation models for QD studies

In the present study, it was difficult to find sets of conditions that produced results that could be applicable to heteroaggregation models, since these models assume heteroaggregation greatly outpaces homoaggregation within an initial mixing period. In this study, if the QDs did not dissolve, they experienced homoaggregation, and vice versa. The only two conditions where dissolution was not an issue were CdSe-CL4 and CdSe-MPA with kaolinite in saline (NaCl). Following the methods of Geitner et al. (2016) and Barton et al. (2014), Eq. (3) (Section 2.9) was plotted and $\alpha\beta B$ was calculated from the slopes of the first minute, where our controls show particle breakup to be negligible (Fig. 7). $\alpha\beta B$ for CdSe-CL4 and kaolinite was 13.5 times that for CdSe-MPA and kaolinite. This difference shows the influence of nanoparticle ligand functional groups on nanoparticle behavior. α was not calculated by itself due to our limited appropriate data set, inconsistent initial removal values, and removals reaching 100% within short periods of time. Since only the simple media composition of 4.7 mM NaCl resulted in calculable measures of attachment efficiency, more work is needed to effectively extract this information from more environmentally relevant media.

4. Conclusions

This work shows that the dynamic nature of ligand-coated nanoparticle behavior in environmentally relevant conditions makes it difficult to isolate heteroaggregation processes from homoaggregation and nanoparticle dissolution, in order to calculate attachment efficiencies. To date, studies of ENM aggregation kinetics have focused on nanoparticles that are relatively stable against ligand detachment and oxidative dissolution, unlike the QDs in the present study. For the

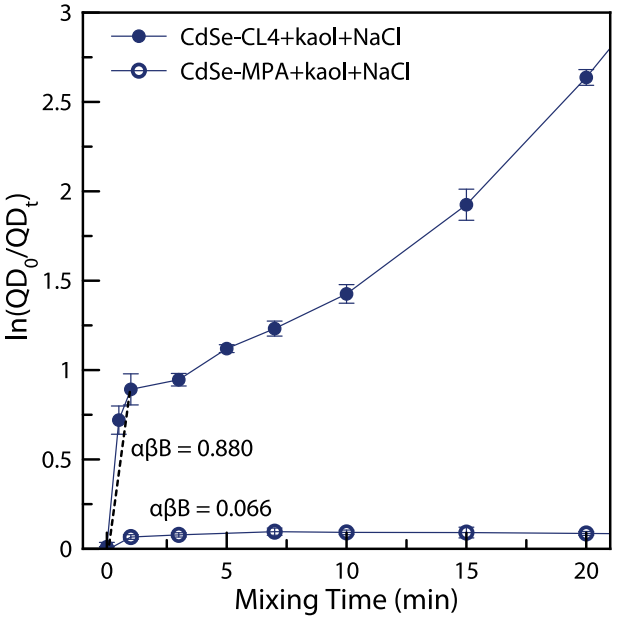

Fig. 7. Natural log plots of QD concentrations (calculated from Cd) where the initial slope of the line is *αβB*. These represent the clay-only portion, where the control values were subtracted from the average values of experiments with clay present. Standard deviations represent triplicate experiments, with the average values taken after calculating the y-axis value.

conditions that favored intact QDs (4.7 mM NaCl), CdSe-CL4 attachment efficiency to kaolinite was over 10 times that for CdSe-MPA. Within 20 min of mixing, 1.6 times more CdSe-CL4 was removed by kaolinite than by montmorillonite, and 2.5 times more than CdSe-MPA by kaolinite. Zeta potentials help explain trends but, as other studies have shown (Espinasse et al., 2018), are limited by many other factors in complex media. Fundamentally, the bond strength and speciation of any ligand coating as measured in the relevant environment is one of the critical determinants of a nanomaterial's fate and mobility as it transitions between systems throughout its lifecycle.

Conflicts of interest

There are no conflicts to declare.

Acknowledgements

Lihui Gao, Tharange Jayarathne, Lorenzo Rossi, and Sabrina Riley assisted with kinetics experiments. Chris Scanlon (Agilent) provided training on low-interference Se measurements by ICP-MS. Ramiro Chavez performed the flash chromatography purification of CL4. Boris Lau and Michael Nguyen (UMass-Amherst) graciously allowed the use of their Malvern Zetasizer. Ron Kent (Navarro) advised on PHREEQC modeling. CAJ and this research were supported by the National Science Foundation under Grant Number NSF CBET-1505718. AMD was supported by the National Center for Advancing Translational Sciences, National Institutes of Health, through BU-CTSI Grant Number 1KL2TR001411. Financial support for MC was provided through the Clare Boothe Luce (CBL) Program from the Henry Luce Foundation.

Appendix A. Supplementary data

Electronic Supplementary Information (ESI) available: An additional file provides selected results from the water chemistry and ion speciation (Ca, Mg, Cd, Se) modeling using PHREEQC, as well as graphs of CdSe-CL4 and montmorillonite in saline and its corresponding control experiment. Supplementary data to this article can be found online at https://doi.org/10.1016/j.impact.2019.01.004.

References

Hines, D., Kamat, P.V., 2014. ACS Appl. Mater. Interfaces 6, 3041–3057.
Accuray Research, L.L.P., 2016. Global Nanotechnology Market Analysis & Trends - Industry Forecast to 2025.
Al-Salim, N., Barraclough, E., Burgess, E., Clothier, B., Deurer, M., Green, S., Malone, L., Weir, G., 2011. Sci. Total Environ. 409, 3237–3248.
Aruguete, D.M., Guest, J.S., Yu, W.W., Love, N.G., Hochella, M.F., 2010. Environ. Chem. 7, 28–35.
Barton, L.E., Therezien, M., Auffan, M., Bottero, J.-Y., Wiesner, M.R., 2014. Environ. Eng. Sci. 31, 421–427.
Butt, H.-J., Graf, K., Kappl, M., 2006. Physics and Chemistry of Interfaces, 2nd ed. Wiley - VCH Verlag GmbH, Weinheim.
Chen, X., Sik, Y., Mohan, D., Pittman, C.U., Dou, X., 2017. Chemosphere 185, 926–933.
Chern, M., Nguyen, T.T.H., Mahler, A.H., Dennis, A.M., 2017. Nanoscale 9, 16446–16458.
Cho, S.J., Maysinger, D., Jain, M., Röder, B., Hackbarth, S., Winnik, F.M., 2007. Langmuir 23, 1974–1980.
Delehanty, J.B., Susumu, K., Manthe, R.L., Algar, W.R., Medintz, I.L., 2012. Anal. Chim. Acta 750, 63–81.
Derjaguin, B., Landau, L.D., 1941. Acta Physicochim. URSS 14, 633–662.
Domingos, R.F., Simon, D.F., Hauser, C., Wilkinson, K.J., 2011. Environ. Sci. Technol. 45, 7664–7669.
Espinasse, B.P., Geitner, N.K., Schierz, A., Therezien, M., Richardson, C.J., Lowry, G.V., Ferguson, L., Wiesner, M.R., 2018. Environ. Sci. Technol. 52, 4072–4078.
Esteve-Turrillas, F.A., Abad-Fuentes, A., 2013. Biosens. Bioelectron. 41, 12–29.
Friedlander, S., 1977. Smoke, Dust and Haze: Fundamentals of Aerosol Dynamics, 2nd ed. Oxford University Press, New York.
Future Markets Inc., 2018. The Global Market for Quantum Dots to 2030.
Geitner, N.K., Marinakos, S.M., Guo, C., O'Brien, N., Wiesner, M.R., 2016. Environ. Sci. Technol. 50, 6663–6669.
Geitner, N.K., O'Brien, N.J., Turner, A.A., Cummins, E.J., Wiesner, M.R., 2017. Environ. Sci. Technol. 51, 13288–13294.
Ghosh, Y., Mangum, B.D., Casson, J.L., Williams, D.J., Htoon, H., Hollingsworth, J.A., 2012. J. Am. Chem. Soc. 134, 9634–9643.
Gupta, V.K., Carrott, P.J.M., Ribeiro Carrott, M.M.L., Suhas, 2009. Crit. Rev. Environ. Sci. Technol. 39, 783–842.
Hendren, C.O., Lowry, G.V., Unrine, J.M., Wiesner, M.R., 2015. Sci. Total Environ. 536, 1029–1037.
Jasieniak, J., Mulvaney, P., 2007. J. Am. Chem. Soc. 129, 2841–2848.
Jasieniak, J., Smith, L., Van Embden, J., Mulvaney, P., 2009. J. Phys. Chem. C 113, 19468–19474.
Jiang, J.Q., Zeng, Z., Pearce, P., 2004. Water Air Soil Pollut. 158, 53–65.
King-Heiden, T.C., Wiecinski, P.N., Mangham, A.N., Metz, K.M., Nesbit, D., Pedersen, J.A., Hamers, R.J., Heideman, W., Peterson, R.E., 2009. Environ. Sci. Technol. 43, 1605–1611.
Lecoanet, H.F., Bottero, J., Wiesner, M.R., 2004. Environ. Sci. Technol. 38, 5164–5169.
Lowry, G.V., Gregory, K.B., Apte, S.C., Lead, J.R., 2012. Environ. Sci. Technol. 46, 6893–6899.
Miller, R., Wesley, B., Norman, P., 1988. United States Geol. Surv. Water-Supply 2311, 3–6.
Mulvihill, M.J., Habas, S.E., Jen-La Plante, I., Wan, J., Mokari, T., 2010. Chem. Mater. 22, 5251–5257.
National Center for Biotechnology Information PubChem compound database, CID 6514. https://pubchem.ncbi.nlm.nih.gov/compound/6514, Accessed date: 27 November 2017.
Industrial hygiene and toxicology. In: Patty, F. (Ed.), Toxicology, 2nd ed. vol. II Interscience Publishers, New York.
Paydary, P., Larese-Casanova, P., 2015. Int. J. Environ. Anal. Chem. 95, 1450–1470.
Priester, J.H., Stoimenov, P.K., Mielke, R.E., Webb, S.M., Ehrhardt, C., Zhang, J.P., Stucky, G.D., Holden, P.A., 2009. Environ. Sci. Technol. 43, 2589–2594.
Quik, J.T.K., van De Meent, D., Koelmans, A.A., 2014. Water Res. 62, 193–201.
Rocha, T.L., Mestre, N.C., Sabóia-Morais, S.M.T., Bebianno, M.J., 2017. Environ. Int. 98, 1–17.
Sen Gupta, S., Bhattacharyya, K.G., 2012. Phys. Chem. Chem. Phys. 14, 6698–6723.
Shambetova, N., Chen, Y., Xu, H., Li, L., Solandt, J., Zhou, Y., Wang, J., Su, H., Brismar, H., Fu, Y., 2016. J. Phys. Chem. C 120, 3519–3529.
von Smoluchowski, M., 1917. Z. Phys. Chem. 92, 129–168.
Stewart, D.T.R., Noguera-Oviedo, K., Lee, V., Banerjee, S., Watson, D.F., Aga, D.S., 2013. Environ. Toxicol. Chem. 32, 1288–1294.
Susumu, K., Oh, E., Delehanty, J.B., Blanco-Canosa, J.B., Johnson, B.J., Jain, V., Hervey, W.J., Algar, W.R., Boeneman, K., Dawson, P.E., Medintz, I.L., 2011. J. Am. Chem. Soc. 133, 9480–9496.
Taylor, J., Kippeny, T., Rosenthal, S.J., 2001. J. Clust. Sci. 12, 571–582.
Tombácz, E., Szekeres, M., 2004. Appl. Clay Sci. 27, 75–94.
Tombácz, E., Szekeres, M., 2006. Appl. Clay Sci. 34, 105–124.
Uddin, M.K., 2017. Chem. Eng. J. 308, 438–462.
United States Environmental Protection Agency, 2002. Methods for Measuring the Acute Toxicity of Effluents and Receiving Waters to Freshwater and Marine Organisms (EPA-821-R-02-012), 5th ed. US EPA, Washington DC.
United States Environmental Protection Agency, 2016. Definition and Procedure for the Determination of the Method Detection Limit, Revision 2 (EPA 821-R-16-006), Washington DC.
Unuabonah, E.I., Guenter, C., Weber, J., Lubahn, S., Taubert, A., 2013. ACS Sustain.

Chem. Eng. 1 (996–973).
Uyusur, B., Darnault, C.J.G., Snee, P.T., Kokën, E., Jacobson, A.R., Wells, R.R., 2010. J. Contam. Hydrol. 118, 184–198.
A. Valizadeh, H. Mikaeili, M. Samiei, S. M. Farkhani and N. Zarghami, 2012, 19–21.
Vasconcelos, I.F., Bunker, B.A., 2007. J. Phys. Chem. C 111, 6753–6762.
Vengris, T., Binkiene, R., Sveikauskaite, A., 2001. Appl. Clay Sci. 18, 183–190.
Verwey, E.J., Overbeek, J.T.G., 1948. Theory of the Stability of Lyophobic Colloids. Elsevier, New York.
Wang, D., Nap, R.J., Lagzi, I., Kowalczyk, B., Han, S., Grzybowski, B.A., Szleifer, I., 2011. J. Am. Chem. Soc. 133, 2192–2197.
Wiecinski, P.N., Metz, K.M., King Heiden, T.C., Louis, K.M., Mangham, A.N., Hamers, R.J., Heideman, W., Peterson, R.E., Pedersen, J.A., 2013. Environ. Sci. Technol. 47, 9132–9139.
Xiao, Y., Ho, K.T., Burgess, R.M., Cashman, M., 2017. Environ. Sci. Technol. 51, 1357–1363.
Yu, W.W., Qu, L., Guo, W., Peng, X., 2003. Chem. Mater. 15, 2854–2860.
Yukselen, Y., Kaya, A., 2003. Water Air Soil Pollut. 145, 155–168.
Zhang, Y., Clapp, A.R., 2011. Sensors 11, 11036–11055.
Zhou, D., Abdel-Fattah, A.I., Keller, A.A., 2012. Environ. Sci. Technol. 46, 7520–7526.